

# Surface-polariton-like waves guided by thin, lossy metal films

J. J. Burke and G. I. Stegeman

*Optical Sciences Center, University of Arizona, Tucson, Arizona 85721*

T. Tamir

*Department of Electrical Engineering and Computer Science, Polytechnic Institute of New York,  
333 Jay Street, Brooklyn, New York 11201*

(Received 5 August 1985)

The dispersion relations are solved for waves guided by a thin, lossy metal film surrounded by media of dielectric constant  $\epsilon_1$  and  $\epsilon_3$ . For symmetric structures ( $\epsilon_1 = \epsilon_3$ ), there are the usual two Fano modes whose velocity and attenuation vary with film thickness. For very thin films, one of these modes can attain multicentimeter propagation distances when  $\lambda > 1 \mu\text{m}$ . In addition, there are two leaky waves which correspond to waves localized at the  $\epsilon_1$  (or  $\epsilon_3$ ) dielectric-metal interface whose fields decay exponentially across the metal film and radiate an angular spectrum of plane waves into  $\epsilon_3$  (or  $\epsilon_1$ , respectively). Both radiative waves can be interpreted as spatial transients, which could have physical significance near a transverse plane. When  $\epsilon_1 \neq \epsilon_3$ , there are still four distinct solutions for a given film thickness, two radiative and two nonradiative. For lossy films, there are always two nonradiative solutions for thick enough films. As the thickness goes to infinity, the four solutions reduce to two waves, each radiative and nonradiative pair becoming degenerate. The physical interpretation of these solutions and their dependence on dielectric constant and wavelength are discussed.

## I. INTRODUCTION

A well-known<sup>1-4</sup> property of materials which exhibit a real negative dielectric constant is their capacity to guide surface polaritons along their boundary with another medium. A classic case is a metal in which such a dielectric constant is a consequence of the coupling of an electromagnetic field to the more or less free (conduction) electrons in the metal.<sup>5,6</sup> An additional consequence of this coupling to the electron gas is that mechanisms which damp the electron gas oscillations, such as Drude damping, also manifest themselves in the dielectric constant in terms of an imaginary component, i.e.,  $\epsilon_m = -\epsilon_R - i\epsilon_I$ .<sup>7</sup> For a semi-infinite metal, this imaginary term leads to a finite propagation distance for surface plasmon polaritons. For thin metal films, there is coupling between the surface polariton waves associated with each boundary, resulting in two mixed modes, called Fano modes, exhibiting dispersion with film thickness.<sup>1,7-9</sup> Their dissipation in the metal ( $\epsilon_I \neq 0$ ) also results in finite propagation distances for these two modes. In this paper we examine in detail the surface polaritons guided by thin metal films. We find a number of features that are characteristic of "spatial transients." Specifically, the usual symmetric and antisymmetric branches each split into a pair of waves, one radiative and the other nonradiative.

The propagation properties of surface plasmon polaritons traveling along the interface between semi-infinite metal and dielectric media have been studied theoretically by many authors.<sup>1,4,7-9</sup> Although the goal of most experiments has been to investigate the surface polaritons confined to single boundaries, in practice it is usually surface plasmons guided by metal films which are studied. Only

in the infrared,<sup>2,10-12</sup>  $\lambda > 10 \mu\text{m}$ , has it been possible to launch surface plasmon polaritons along a single interface, propagate them a useful distance and then couple them back out into free-space radiation fields. For regions where the dispersion curves depart from the light line, i.e., as  $\omega \rightarrow \omega_p/\sqrt{2}$ , various electron-loss techniques<sup>13</sup> have been used to study surface plasmons. Gratings<sup>14</sup> have also been widely used to excite surface plasmon polaritons. Probably the most popular experimental technique has been attenuated total reflection (ATR).<sup>4</sup> Light incident in a high refractive index medium, usually a prism, is tunneled via evanescent fields across a gap or a metal film to excite surface plasmon polaritons on the metal interface opposite to the high index medium. This approach was usually used to study films  $> 350 \text{ \AA}$  thick<sup>15-24</sup> in structures in which the index difference between the media bounding the metal film is large.

Most of the theoretical studies<sup>7-9,19-21</sup> of surface polaritons guided by thin metal films have concentrated on lossless metals, usually modeled by a free-electron gas. In that case, there are two modes guided by the film, one symmetric and one antisymmetric with respect to their field distributions. Here by symmetric we mean that the transverse electric field does not exhibit a zero inside the metal film—conversely the antisymmetric mode has a zero in its transverse electric field inside the film. [Our terminology coincides with that of integrated optics,<sup>25</sup> but is opposite to the usual solid-state version, which deals with the symmetries of the charge (not field) distributions.] If  $\epsilon_I = 0$ , both modes are lossless as long as their wave vector is larger than that required for plane waves traveling parallel to the surface in the higher index medium. For  $\epsilon_I > 0$ , both modes exhibit loss. For small

enough differences between the dielectric constants of the media bounding the film, the attenuation of the lower surface polariton branch, the symmetric one, decreases to zero as the wave vector approaches that of plane waves in the low index medium.<sup>26,27</sup>

Recently<sup>16,20,24,28-31</sup> the surface polaritons on both branches have been investigated experimentally for very thin metal films (down to 100 Å thick). The highly damped surface polaritons on the upper branch have been observed in highly asymmetric sample structures, i.e., large difference between the refractive indices of the media on either side of the metal film.<sup>16,20,24</sup> For almost symmetric structures, both the symmetric (lower branch) and antisymmetric (upper branch) modes have been observed and the decrease in the attenuation of the symmetric mode with film thickness verified.<sup>28-31</sup>

There have been previous indications that the interpretation of the waves guided by thin metal films is not complete, or fully understood. By using an additional film to effectively increase the refractive index on one side of the metal film, Buckman and Kuo<sup>20</sup> predicted, for their experimental conditions, the usual mixed symmetric and antisymmetric mode, and in addition what appeared to be an extra mode strongly confined to one of the metal surfaces. Recently Ferguson *et al.*<sup>32</sup> predicted a third wave for an air-metal-glass geometry. In addition to a leaky Fano mode, they found a solution which corresponds to a bound wave above a cutoff thickness, and to a growing wave below cutoff. The solution at the cutoff thickness is strongly reminiscent of a Brewster field<sup>1,32</sup> in that an incident plane wave is totally absorbed by the structure.

In the work reported here we find a total of four solutions to the dispersion relations. There are always two leaky (radiative) wave solutions. For thick enough films there are also two nonradiative waves; below some cutoff thickness one of these becomes a growing wave solution. As the film thickness goes to infinity, the solutions form degenerate pairs, one radiative and one nonradiative wave in each of the pairs.

The purpose of this paper is to discuss these solutions in detail, offer physical interpretations, and analyze their dependence on the dielectric constants and wavelength. (Preliminary results of this investigation have already been reported in letter form.<sup>33</sup>) Towards this goal, this paper is arranged as follows. In Sec. II we briefly summarize the dispersion relations being solved. Sections III and IV deal with the solutions for a symmetric ( $\epsilon_1 = \epsilon_3$ ) and asymmetric ( $\epsilon_1 > \epsilon_3$ ) structure, respectively, at the fixed wavelength  $\lambda = 0.63 \mu\text{m}$  (He-Ne laser). The wavelength dependence of the radiative wave solutions is presented in Sec. V. In the last section we present a discussion of the wave solutions, whether they can be launched or not, including a suggestion for "end-fire" techniques, and how their existence may impact on a variety of surface plasmon polariton phenomena.

## II. DISPERSION RELATIONS

The geometry which we analyze is shown in the inset of Fig. 1. A metal film of variable thickness  $h$  and dielectric constant  $\epsilon_m = -\epsilon_R - i\epsilon_I$  is bounded by two dielectric

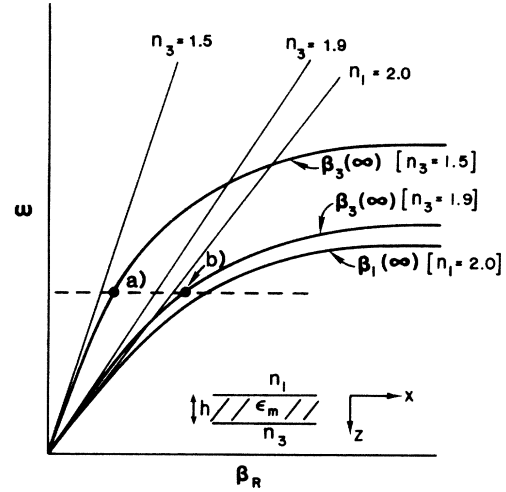


FIG. 1. Dispersion curves  $\beta(\infty)$  for surface-plasmon polaritons propagating along the  $\epsilon_1$ - $\epsilon_m$  and  $\epsilon_3$ - $\epsilon_m$  boundaries for the geometry shown in the inset at  $h \rightarrow \infty$ . The points (a) and (b) at the same frequency lie in the leaky and bound mode regions, respectively, of the light line  $(\epsilon_1)^{1/2} = 2.0$ .

media characterized by  $\epsilon_1$  and  $\epsilon_3$  with  $\epsilon_1 > \epsilon_3$ . For isotropic adjoining media, the surface polariton waves are transverse magnetic in nature, and can best be described by their magnetic fields which lie in the plane of the surface. For waves propagating along the  $x$  axis with  $z$  normal to the surfaces

$$\mathbf{H} = \hat{\mathbf{j}} f(z) C \exp[i(\omega t - \beta x)], \quad (1)$$

where  $\beta = \beta_R - i\beta_I$  is the complex propagation constant parallel to the surface, and  $f(z)$  describes the depth dependence of the magnetic field.  $C$  is a normalization constant chosen so that the wave carries one watt of power per meter of wave front (along the  $y$  axis). The wave energy propagates the distance  $0.5\beta_I^{-1}$  along the surface and the losses can be both dissipative and radiative. As usual, the electric field components can be evaluated from Maxwell's equations, i.e.,

$$E_x = \frac{i}{\omega\epsilon_0\epsilon} \frac{\partial H_y}{\partial z}, \quad E_z = -\frac{\beta}{\omega\epsilon_0\epsilon} H_y. \quad (2)$$

We write the depth distributions in the form

$$\epsilon_1: f(z) = e^{S_1 z}, \quad z < 0 \quad (3)$$

$$\epsilon_m: f(z) = \cosh(S_2 z) + \frac{S_1 \epsilon_m}{S_2 \epsilon_1} \sinh(S_2 z), \quad 0 > z > h \quad (4)$$

$$\epsilon_3: f(z) = \begin{cases} \cosh(S_2 h) \\ + \frac{S_1 \epsilon_m}{S_2 \epsilon_1} \sin(S_2 h) \end{cases} e^{-S_3(z-h)}, \quad z > h \quad (5)$$

where  $S_1$ ,  $S_2$ , and  $S_3$  are obtained from the wave equation as

$$\begin{aligned} S_1^2 &= \beta^2 - \epsilon_1 k_0^2, \\ S_2^2 &= \beta^2 - \epsilon_m k_0^2, \\ S_3^2 &= \beta^2 - \epsilon_3 k_0^2. \end{aligned} \quad (6)$$

By writing the fields in the form of Eqs. (3)–(5), we ensure that the tangential magnetic fields are continuous at  $z=0$  and  $z=h$ . Continuity of the tangential  $E$  field at  $z=h$  leads to the dispersion relation

$$\tanh(S_2 h) (\epsilon_1 \epsilon_3 S_2^2 + \epsilon_m^2 S_1 S_3) + [S_2 (\epsilon_1 S_3 + \epsilon_3 S_1) \epsilon_m] = 0 \quad (7)$$

which must be satisfied for a solution to exist.

The solutions to Eq. (7) are well known when the film thickness  $h$  is much greater than the classical skin depth  $c/\omega_p$ , where  $\omega_p$  is the plasma frequency. In this limit  $\tanh(S_2 h) \rightarrow 1$  and Eq. (7) becomes

$$(S_1 \epsilon_m + S_2 \epsilon_1)(S_3 \epsilon_m + S_2 \epsilon_3) = 0, \quad (8a)$$

which leads to

$$S_1 \epsilon_m = -S_2 \epsilon_1, \quad S_3 \epsilon_m = -S_2 \epsilon_3. \quad (8b)$$

Assuming that  $\text{real}[S_i] > 0$ , that is the fields are bound in all of the media, the solutions consist of decoupled surface-plasmon polaritons propagating along the  $\epsilon_1$ – $\epsilon_m$  and  $\epsilon_3$ – $\epsilon_m$  interfaces with the dispersion relations

$$\beta_1(\infty) = (\epsilon_1)^{1/2} k_0 \left[ \frac{\epsilon_m}{\epsilon_m + \epsilon_1} \right]^{1/2} \quad (9a)$$

and

$$\beta_3(\infty) = (\epsilon_3)^{1/2} k_0 \left[ \frac{\epsilon_m}{\epsilon_m + \epsilon_3} \right]^{1/2}, \quad (9b)$$

respectively. For convenience we shall label these modes  $\text{SP}_1$  and  $\text{SP}_3$ , respectively. Assuming  $\beta_R \gg \beta_I$  and complex  $\epsilon_m$ ,

$$\beta_{iR}(\infty) \simeq (\epsilon_i)^{1/2} k_0 \left[ \frac{\epsilon_R^2 - \epsilon_R \epsilon_i + \epsilon_i^2}{|\epsilon_m + \epsilon_i|^2} \right]^{1/2}, \quad (10a)$$

$$\beta_{iI}(\infty) = \frac{1}{2} \frac{\epsilon_i^2 \epsilon_I}{\beta_{iR}} \frac{k_0^2}{|\epsilon_m + \epsilon_i|^2}, \quad (10b)$$

which is a useful result since the thin metal modes must approach these values asymptotically for very thick films. In Fig. 1 we show the dispersion relations for  $\epsilon_I = 0$ ,  $(\epsilon_1)^{1/2} = 2.0$ , and  $(\epsilon_3)^{1/2} = 1.9$  and 1.5, as well as the “light” lines for each medium, which correspond to  $\beta_R = \sqrt{\epsilon} \omega/c$ . Note that  $\beta_R > \sqrt{\epsilon} \omega/c$  for the semi-infinite media surface plasmon polaritons and therefore those modes are nonradiative, or bound, because  $S_R^2 = \beta_R^2 - \epsilon k_0^2 > 0$ . The dashed line corresponds to the frequency of the He-Ne laser.

It will be useful later to note that there is a second set of solutions for this case which are rejected because they do not correspond to guided waves. The dispersion relations are still valid for  $\text{real}[S_i] < 0$ , which correspond to fields which grow exponentially with distance from the interface. Hence the two semi-infinite media case actually

consists of two solutions, one of which is rejected as unphysical.

For a finite film thickness, it is generally accepted that the two allowed semi-infinite media modes are coupled and the values of  $\beta$  for the two waves depend on film thickness. If  $(\epsilon_1)^{1/2} = (\epsilon_3)^{1/2} = 2.0$ , the modes continue to lie to the right of the light line and remain nonradiative for all film thicknesses. For  $(\epsilon_1)^{1/2} = 2.0$  and  $(\epsilon_3)^{1/2} = 1.9$  [point (b) in Fig. 1], and for very thick films one would expect both modes to remain nonradiative, i.e., to lie to the right of the light line. As we shall see later for thin films, the mode associated with field localization at the  $\epsilon_3$ – $\epsilon_m$  interface (for large  $h$ ) actually crosses the  $\epsilon_1$ – $\epsilon_m$  light line and becomes leaky (radiative) into medium  $\epsilon_1$ . If  $(\epsilon_1)^{1/2} = 2.0$  and  $(\epsilon_3)^{1/2} = 1.5$  [point (a) in Fig. 1], one mode [corresponding to  $\beta_1(\infty)$  as  $h \rightarrow \infty$ ] remains nonradiative and the second [ $\beta_3(\infty)$  as  $h \rightarrow \infty$ ] is radiative for all film thickness. These assignments, nonradiative or radiative, are usually made on the basis of whether or not  $S^2 = \beta^2 - \epsilon k_0^2$  is positive in both media. If  $\epsilon k_0^2 > \beta^2$ ,  $S^2 < 0$ ,  $S$  is imaginary and the field in that medium corresponds to a plane wave radiating away from the metal boundary.

In the preceding discussion of films we have carefully avoided the question of complex refractive indices in one of the three media, more specifically, dissipation in the metal via an  $\epsilon_I \neq 0$ . For a real metal,  $\epsilon_I > 0$ , which leads directly to a complex wave vector  $\beta$ . Consequently,  $S_1$  and  $S_3$  are also complex numbers<sup>34–37</sup> which we write in the form

$$S_1 = S_{1R} - iS_{1I}; \quad S_3 = S_{3R} - iS_{3I}. \quad (11)$$

In the analysis that follows we shall explore solutions to the dispersion relations for the full spectrum of possible signs for  $S_1$  and  $S_3$ , i.e.,  $\pm S_1$  and  $\pm S_3$  taken in all possible combinations. For convenience, we have found all solutions for which  $\beta_R > 0$  but, it is clear from Eqs. (6) that these solutions appear in pairs, i.e., if  $\beta_s$  is a solution, then  $-\beta_s$  is also a solution. Our criteria for accepting or rejecting solutions will be based on whether the field distributions correspond to physically acceptable guided waves, that is waves whose energy is highly localized in one of the bounding media.

Before closing this section, we wish to emphasize again that even in the case of  $\epsilon_I = 0$ , the dispersion relation, Eq. (7), is still valid. That is, all valid solutions, independent of their radiative or nonradiative status, must satisfy Eq. (7). Conversely, all solutions to Eq. (7) correspond to real waves as long as they can be justified on physical grounds. We make these points because we shall later discuss valid solutions to Eq. (7) which initially appear to violate the preceding discussion of the role played by the light line. Under closer inspection, it will be shown that the underlying physics dictates that these waves may have a physical interpretation.

### III. WAVES GUIDED BY SYMMETRIC STRUCTURES

The transcendental set of Eqs. (6) and (7) were solved numerically on a computer. Rather than actual zeros for Eq. (7) we obtained minima for all of the model solutions

which were  $10^{-7}$ – $10^{-9}$  below the values of Eq. (7) away from the minima. The dielectric constant of silver films at  $\lambda=0.633 \mu\text{m}$  was assumed to be  $\epsilon_m = -19 - 0.53i$ .

In a symmetric structure ( $\epsilon_1 = \epsilon_3$ ), the possibilities are  $\pm S_1 = \pm S_3$ . For the choice  $-S_1$  and  $-S_3$  with  $-S_1 = -S_3$ , the fields grow exponentially away from the film with wave fronts tilted to carry energy away from the film. An exponentially growing field perpendicular to the metal-dielectric interfaces is the signature of a leaky (radiative)<sup>34–37</sup> wave, which will be discussed in more detail in the next section.

The solutions which occur for  $S_1 = S_3 = S_{1R} - iS_{1I}$  are the extensions of the usual Fano modes with loss included. The fields decay exponentially into both  $\epsilon_1$  and  $\epsilon_3$ , and the wave fronts are tilted in towards the metal film. This tilt removes energy from the dielectric media (for dissipation in the film) as the wave attenuates with propagation distance. Thus the physically important solutions correspond to nonradiative waves.

The dispersion relations were solved at  $\lambda=0.633 \mu\text{m}$  for this case and the results are shown in Fig. 2. For  $\epsilon_I = 0$ , the modes are lossless; for  $\epsilon_I = 0.53$ , the imaginary part of  $\beta$  is plotted in Fig. 2. Because of the geometrical symmetry, the field distributions must be either symmetric or antisymmetric with respect to the center of the metal film. The upper branch [ $\beta > \beta(\infty)$ ] is antisymmetric and the lower branch is symmetric.

The variation of  $\beta_I$  with film thickness can be understood in terms of the dispersion in  $\beta_R$  and the decay constants  $S_1 = S_3$ . For the antisymmetric mode, the increase in  $\beta_R$  with decreasing  $h$  leads to an increase in  $S_1$  [Eqs. (6)] and hence progressively more of the mode energy is carried (and dissipated) in the metal. Therefore  $\beta_I$  increases as  $h$  decreases. Conversely for the symmetric case as  $\beta_R \rightarrow (\epsilon_1)^{1/2}k_0$  (Fig. 2) the fields penetrate progressively deeper into the adjacent media, and dissipation in the metal is reduced. As  $h \rightarrow 0$ , the fields in the  $\epsilon_1$  and  $\epsilon_3$  media approach those of a plane wave and the loss goes to zero. This was first pointed out by Fukui *et al.*<sup>26</sup> If there is loss in the bounding media (via a complex refractive index  $n - i\kappa$ ), the attenuation as  $h \rightarrow 0$  is asymptotic to plane-wave loss in these media (Fig. 2).

The symmetric (lower branch) mode is of potential practical interest because of the long propagation distances possible with thin metal films. Since it is difficult to fabricate continuous metal films of silver, copper, etc., for film thicknesses less than  $100 \text{ \AA}$ , we assume that a minimum film thickness of  $150 \text{ \AA}$  is required for guiding. For the dielectric constants  $(\epsilon_1)^{1/2} = (\epsilon_3)^{1/2} = 2.0$ , the propagation distance is  $140 \mu\text{m}$  for  $h = 150 \text{ \AA}$ . According to Eq. (10) for waves at the interface between two semi-infinite media, the  $h \rightarrow \infty$  loss is proportional to  $\epsilon_1^{3/2}$  and hence attenuation can be reduced by using lower refractive index media. This is verified for the thin film case in Fig. 3. For  $(\epsilon_1)^{1/2} = 1.5$ , the propagation distance increases to  $610 \mu\text{m}$ , 40 times further than for surface plasmons along the interface between semi-infinite silver and a medium of index 1.5. Such increases have been seen experimentally.<sup>28–31</sup>

Solutions to the dispersion relations are also possible for  $S_1 = -S_3$  and  $-S_1 = S_3$ . From Eq. (7) this occurs for

$\beta = \beta(\infty)$  in both cases. For  $S_1 > 0$ , the field in  $\epsilon_1$  and the metal is identical to that guided by the interface between a semi-infinite metal and the dielectric  $\epsilon_1$ . The field in  $\epsilon_3$  grows exponentially with distance from the interface, which is a characteristic of a leaky wave.<sup>34–36</sup> The loss coefficient is  $\beta_I = \beta_{II}(\infty)$  and the dissipation in the metal, which is reduced from the  $\beta_{II}(\infty)$  case because of the finite thickness of the metal film, is exactly compensated for by the radiation loss term. We shall discuss the ramifications of these solutions in more detail in Sec. IV.

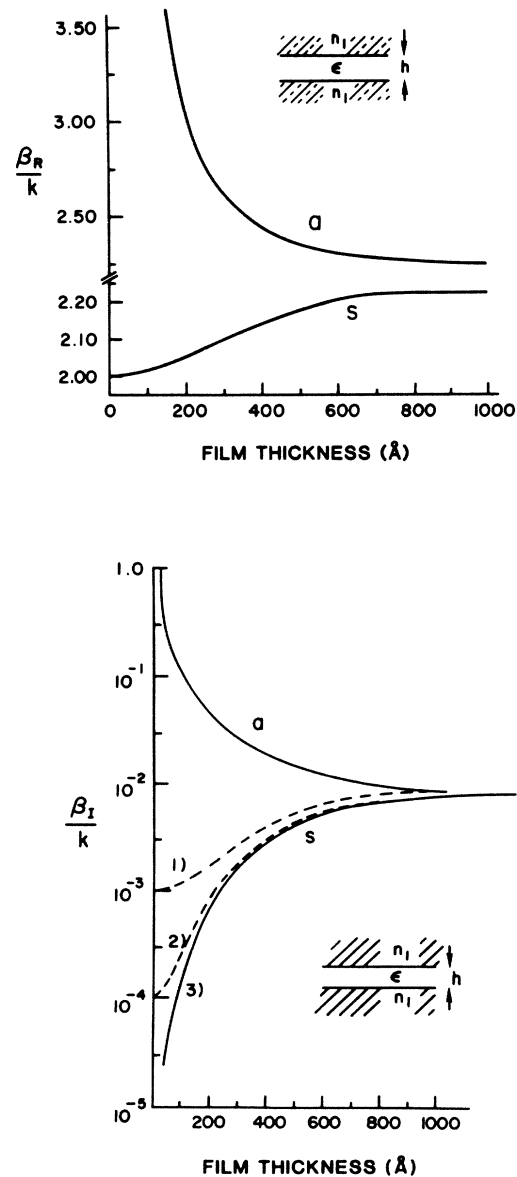


FIG. 2. Normalized complex propagation wave vector  $\beta$  as a function of film thickness for the symmetric structure with  $(\epsilon_1)^{1/2} = 2.0$ .  $a$  and  $s$  refer to the antisymmetric and symmetric waves, respectively. (1)  $(\epsilon_1)^{1/2} = 2.0 - 0.001i$ , (2)  $(\epsilon_1)^{1/2} = 2.0 - 0.0001i$ , and (3)  $(\epsilon_1)^{1/2} = 2.0$ ,  $\epsilon_m = -19 - 0.53i$ .

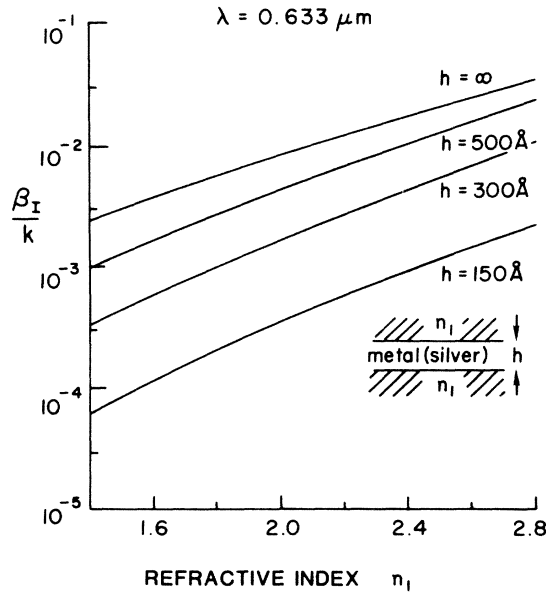


FIG. 3. Variation in normalized attenuation with refractive index  $\sqrt{\epsilon}$  for a symmetric structure ( $\epsilon_1 = \epsilon_3$ ) for different film thicknesses ( $\lambda = 0.633 \mu\text{m}$ ,  $\epsilon_m = -19 - 0.53i$ ).

#### IV. WAVES GUIDED BY ASYMMETRIC STUDIES: FIXED FREQUENCY

##### A. Types of solutions

There are also four interesting solutions to Eq. (7) for the asymmetric structure. We find that one antisymmetric mode is always obtained. The "symmetric" solutions are of two types, radiative and nonradiative and typical amplitude-wave-front sketches of the fields are shown in Fig. 4. For the nonradiative case (upper left), the fields in the dielectric decay exponentially away from the film and the wave fronts are tilted into the metal film, as required, in order to remove energy from the dielectric media (for dissipation in the metal) as the wave attenuates with propagation distance.

Two leaky (radiative) solutions are always found, just as in the symmetric case. However, because there is no

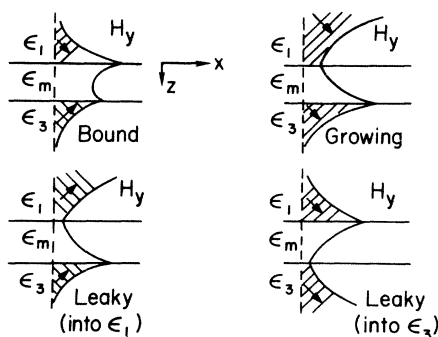


FIG. 4. Field distributions associated with bound, leaky, and growing modes guided by thin metal films. The arrows indicate energy flow in the dielectrics.

longer symmetry in the structure, the degeneracy between the solutions is lifted. The wave energy is localized in one of the dielectrics, say  $\epsilon_1$ , at that dielectric-metal interface ( $\epsilon_1 - \epsilon_m$ ). The wave amplitude decays exponentially across the film, and then grows exponentially into the other dielectric medium,  $\epsilon_3$  in this case. In the  $\epsilon_1$  medium, the wave fronts are tilted towards the film to supply energy from  $\epsilon_1$  for both dissipation in the metal, and radiation into  $\epsilon_3$ . The analogous case of localization in  $\epsilon_3$ , and radiation into  $\epsilon_1$  also occurs.

Fields which grow exponentially away from the boundaries are a signature of leaky waves,<sup>34-36</sup> whose characteristics are perhaps not widely known in the solid-state physics community. They only have meaning in a limited region of space above the film and require some transverse plane (say  $x=0$ ) containing an effective source that launches a localized wave in one dielectric near its metal-dielectric boundary. The field decays across the metal and couples to radiation fields in the opposite dielectric. As shown for a specific example in Fig. 5, for any plane  $x > 0$  the wave radiates at some angle  $\theta$  into medium  $\epsilon_1$ , and the  $\epsilon_1$  field amplitude grows exponentially for only a finite distance  $z$ , which is a function of  $x$  and  $\theta$ . In this sense, the solutions do not violate boundary conditions as  $z \rightarrow -\infty$ , and in fact have the characteristics of spatial transients.<sup>36</sup> This interpretation requires that the effective distance into  $\epsilon_1$ , i.e.,  $S_{IR}^{-1}$ , must equal  $\beta_I^{-1} \tan \theta$ , where  $\theta$  is the wave-front tilt defined by  $\tan \theta = S_{II}/\beta_R$ , that is  $S_{IR}S_{II} = \beta_R\beta_I$ . This condition is simply the imaginary part of the first equation of (6) and is trivially satisfied by these solutions.

When such a leaky wave is excited at  $x=0$ , the local, exponentially increasing fields near the structure do not provide a useful description for the radiation fields in medium  $\epsilon_1$  (the Fraunhofer region). Instead, it is more useful to replace the local  $\epsilon_1$  fields by an appropriately phased sheet of equivalent current in the  $x$ - $y$  plane for  $x \geq 0$ . The radiation field may then be viewed as that associated with a finite (along  $x$ ) aperture. For fields radiated at an angle  $\theta$  relative to the surface, the angular spectrum of the radiated plane waves is

$$F(\theta) = \sin \theta \int_{-\infty}^{\infty} dx \exp[-i(\beta_R - \sqrt{\epsilon} k_0 \cos \theta) - \beta_I x], \quad (12)$$

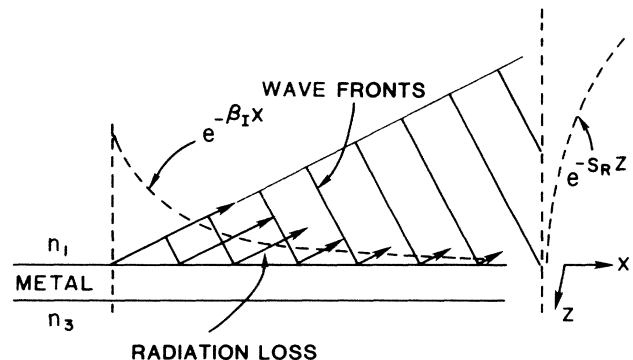


FIG. 5. Schematic of how a radiating surface-polariton wave which decays along the  $x$  axis as  $\exp[-\beta_I x]$  produces an exponentially increasing field in a plane normal to the  $x$  axis.

which gives for the radiated power

$$|F(\theta)|^2 = \frac{\sin^2 \theta}{(\beta_R - \sqrt{\epsilon} k_0 \cos \theta)^2 + \beta_I^2}. \quad (13)$$

For  $\beta_R < \sqrt{\epsilon} k_0$ , there is a well-defined peak in  $|F(\theta)|^2$  at  $\theta = \cos^{-1}(\beta_R / \sqrt{\epsilon} k_0)$  with an angular breadth proportional to  $\beta_I$ . If  $\sqrt{\epsilon} k_0 < \beta_R$ , radiation occurs over a large range of directions; thus leaky waves can still exist on the side of the "light line" usually associated with bound (nonradiative) modes.

The wave attenuation due to radiation loss can be estimated from the solutions by calculating the Poynting vector for energy leaving, for example, the  $\epsilon_1$ - $\epsilon_m$  boundary. Thus the decrease in surface wave power due to radiation loss, per meter of wave front, is given by

$$\frac{dP}{dx} = -\frac{1}{2} C^2 \frac{S_{1I}}{k_0 c \epsilon_0 \epsilon_1} P = -2\beta_I' P, \quad (14)$$

where  $\beta_I'$  is the field-amplitude attenuation due to radiation loss.

We now briefly discuss the nature of the growing wave solutions which were also found by Ferguson *et al.*<sup>32</sup> In this case, the field amplitude grows both with propagation distance as  $\exp(\beta_I x)$ , and into one of the dielectrics as  $\exp(S_R z)$ . Since the wave-front tilt is into the film (as opposed to away from it for leaky waves), these waves are dependent on externally incident fields supplying energy to make the total wave amplitude grow.

#### B. Solutions for $(\epsilon_1)^{1/2} = 2.0$ , $(\epsilon_3)^{1/2} = 1.5$

We now evaluate the dispersion relations numerically for two sets of material parameters. From Fig. 1 we expect that the waves for  $\beta_3(\infty) < (\epsilon_1)^{1/2} k_0$  will be different from those for  $\beta_3(\infty) > (\epsilon_1)^{1/2} k_0$ . The former corresponds to the semi-infinite surface-plasmon curve SP<sub>3</sub> crossing the  $\epsilon_1$  medium light line, the case that we now consider.

The numerical solutions for  $\beta_R$  and  $\beta_I$  are shown in Fig. 6. The curves labeled  $a_b$  (antisymmetric, nonradiative) and  $s_l$  (symmetric, leaky) are commonly called Fano<sup>1</sup> modes and have been discussed in detail previously<sup>19-21</sup> usually in connection with ATR experiments. The symmetric wave is attenuated both by dissipation in the film and radiation loss into  $\epsilon_1$ . It is characterized by  $\beta_R \approx \beta_3(\infty)$ , almost independent of film thickness and exhibits little dispersion until  $\beta_I'$  becomes of the order of a wavelength. This wave has essentially all the characteristics of the SP<sub>3</sub> surface plasmon. It loses energy via radiation fields generated into the  $\epsilon_1$  medium and the radiation pattern is highly directional because  $\beta < (\epsilon_1)^{1/2} k_0$ .

The branch labeled  $a_l$  has all the characteristics of a surface plasmon which is localized at the  $\epsilon_1$ - $\epsilon_m$  interface [SP<sub>1</sub>], it decays exponentially across the metal film, and it couples to radiation fields in  $\epsilon_3$ . Because of dissipation in the metal,  $\beta_I > 0$  and, as indicated by Eq. (13), the angular spectrum of the radiation fields in  $\epsilon_3$  is broad. Note that the attenuation of this wave is less than that of the antisymmetric bound mode, despite the radiation losses and its spatial transient nature. This occurs because the metal

film which is highly dissipative, carries more of the antisymmetric mode energy as the film thickness decreases. As the film thickness increases, the  $a_b$  and  $a_l$  branches become degenerate, as required for an interface between semi-infinite media, which supports only one mode localized at the  $\epsilon_1$ - $\epsilon_m$  boundary. To the best of our knowledge, the  $a_l$  branch has not been discussed before.

The component of the leaky (radiative) wave attenuation due to the radiation loss is plotted in Fig. 7. The straight lines obtained for both cases in this lin-log plot are verification of the exponentially decaying nature of the wave fields in the metal film. For this  $a_l$  branch, the radiation loss is small, as expected, because this solution lies on the nonradiative side of the  $\epsilon_3$  light line.

The fourth branch,  $s_b$ , was reported previously by Ferguson *et al.*<sup>32</sup> For thicknesses greater than  $h_{c0} = 520$  Å, it corresponds to a bound (nonradiative) wave, and below  $h_{c0}$ , the wave amplitude grows with propagation distance. Just at  $h_{c0}$ , there is a change in the  $\epsilon_1$  field from exponentially growing to exponentially decaying into  $\epsilon_1$ . At  $h_{c0}$ , this solution corresponds to plane waves incident from  $\epsilon_1$  which feed a resonance localized at the  $\epsilon_3$ - $\epsilon_m$  boundary.

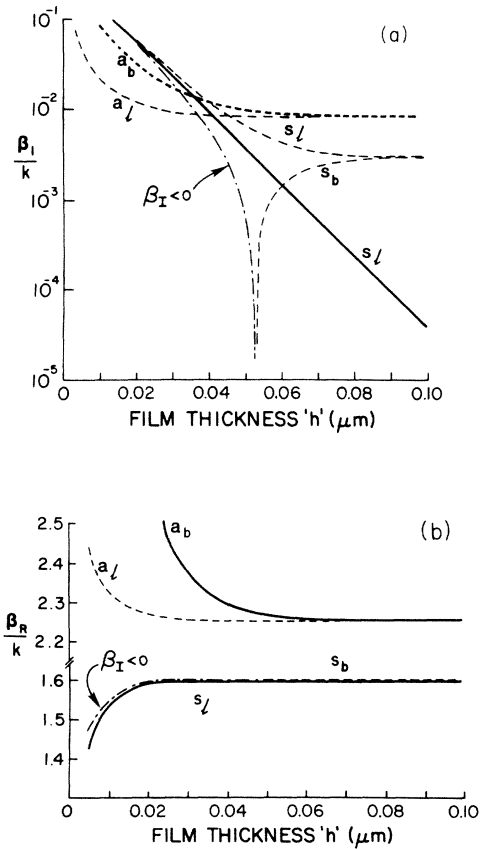


FIG. 6. Solutions for an asymmetric structure with  $(\epsilon_1)^{1/2} = 2.0$  and  $\sqrt{\epsilon} = 1.5$  as a function of film thickness with  $\epsilon_m = -19 - 0.53i$ . The upper (antisymmetric) and lower (symmetric) branches are labeled  $a$  and  $s$ . The subscripts  $b$  and  $L$  indicate bound (nonradiative) and leaky (radiative) waves respectively. The solid lines pertain to  $\epsilon_I = 0$  as well as  $\epsilon_I = 0.53$  for  $\beta_R$ .

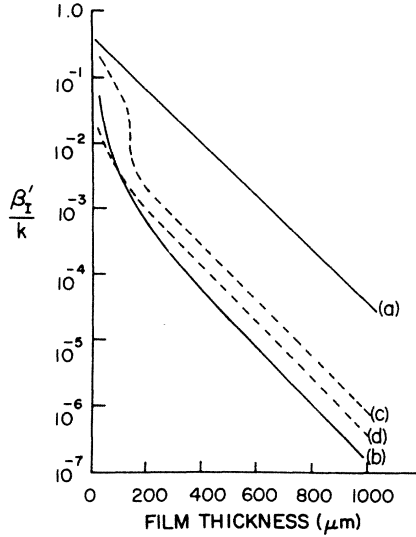


FIG. 7. Attenuation due to radiation loss by surface-plasmon polaritons localized at the metal-dielectric interface opposite to the dielectric medium into which loss occurs (a) for  $(\epsilon_1)^{1/2}=2.0$ ,  $(\epsilon_3)^{1/2}=1.5$ , wave leaking into  $\epsilon_1$ ; (b)  $(\epsilon_1)^{1/2}=2.0$ ,  $(\epsilon_3)^{1/2}=1.5$ , wave leaking into  $\epsilon_3$ ; (c)  $(\epsilon_1)^{1/2}=2.0$ ,  $(\epsilon_3)^{1/2}=1.9$ , wave leaking into  $\epsilon_1$ ; (d)  $(\epsilon_1)^{1/2}=2.0$ ,  $(\epsilon_3)^{1/2}=1.9$ , wave leaking into  $\epsilon_3$ .

This is a steady-state situation in which the incident field energy is totally dissipated in the metal and  $\beta_I=0$ . In the parlance of recent literature this is a Brewster mode at  $h_{c0}$ . Away from  $h_{c0}$ , the “no reflection” condition requires a superposition of incident plane waves, properly phased and properly contoured in amplitude along the  $z$  axis. For  $h > h_{c0}$  less energy is supplied through the  $\epsilon_1$ - $\epsilon_m$  boundary to the resonance than is dissipated in the metal, and the solution attenuates with propagation distance. Because  $\beta_I\beta_R = S_{I1}S_{1R}$ , this requires an exponentially decaying field into  $\epsilon_1$ . For  $h < h_{c0}$ , the rate of energy flux from  $\epsilon_1$  into the wave is greater than the dissipation in the metal and the wave grows.

### C. Solutions for $(\epsilon_1)^{1/2}=2.0$ , $(\epsilon_3)^{1/2}=1.9$

We now examine the solutions for the case  $\beta_3(\infty) > (\epsilon_1)^{1/2}k_0$ . For the semi-infinite media case, the modes all lie on the nonradiative side of the light lines (Fig. 1). As in the previous cases, four distinct solutions are obtained for every film thickness (see Fig. 8). There are two nonradiative modes for  $h$  greater than a cutoff thickness,  $h_{c0}$ , and one for  $h_{c0} > h$ . For all values  $h$  there are two radiative waves.

The two upper branch solutions are similar to those discussed for the previous  $[(\epsilon_3)^{1/2}=1.5]$  case. The  $a_b$  branch is an antisymmetric mode termed Fano in the literature,<sup>1</sup> whose attenuation increases dramatically with decreasing film thickness as more of the wave energy is carried by the metal. The leaky wave  $a_l$  has all the characteristics of a semi-infinite medium surface-plasmon polariton localized at the  $\epsilon_1$ - $\epsilon_m$  boundary, whose field decays exponentially across the film, coupling to a broad angular spectrum of radiation fields in  $\epsilon_3$ . Since the difference

$\beta_R - (\epsilon_3)^{1/2}k_0$  is smaller than for the  $(\epsilon_3)^{1/2}=1.5$  case, the coupling to radiation modes is stronger than for the  $(\epsilon_3)^{1/2}=1.5$  case, see Eq. (13). This is illustrated numerically in Fig. 7. Finally, the attenuation of the leaky wave is smaller than that of the nonradiative waves, as noted in the previous example and for the same reason as discussed there.

There is also a leaky wave solution associated with a surface plasmon polariton localized at the  $\epsilon_3$ - $\epsilon_m$  interface. It radiates into medium  $\epsilon_1$  via field tunneling (exponential decay) across the metal film. This solution is especially interesting because its dispersion with thickness moves it across the  $\epsilon_1$  light line. For very thin films  $(\epsilon_1)^{1/2}k_0 > \beta_R$  and the leaky wave radiation pattern becomes highly directional and radiation loss dominates the wave attenuation (Fig. 7). For  $(\epsilon_1)^{1/2}k_0 < \beta_R$ , i.e., on the nonradiative side of the  $\epsilon_1$  light line, the radiation loss decreases quickly with increasing film thickness. Under closer scrutiny, the transition occurs for  $\beta_R$  greater than  $(\epsilon_1)^{1/2}k_0$  (Figs. 7 and 8), which indicates that Eq. (13) is only an approximation. (This change in wave character persists even in the limit  $\epsilon_I \rightarrow 0$ .)

The behavior of the nonradiative lower branch is similar to that discussed previously for the case  $(\epsilon_3)^{1/2}=1.5$ . For  $h > h_{c0}$ , the solution exhibits a symmetric type of

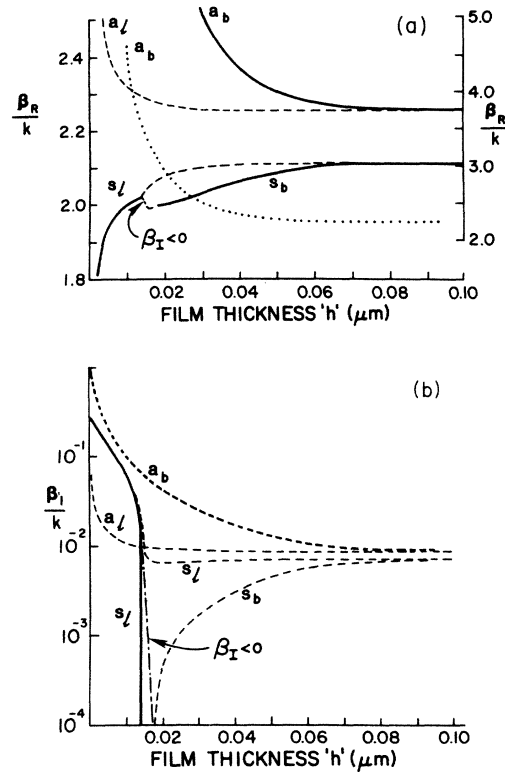


FIG. 8. Modal solutions for an asymmetric structure with  $(\epsilon_1)^{1/2}=2.0$  and  $(\epsilon_3)^{1/2}=1.9$  as a function of film thickness. The upper (antisymmetric) and lower (symmetric) branches are labeled  $a$  and  $s$ . The subscripts  $b$  and  $l$  indicate bound (nonradiative) and leaky (radiative) waves, respectively.  $\epsilon_m = -19 - 0.53i$ . The solid lines characterize the case  $\epsilon_I=0$ , as well as  $\epsilon_I=0.53$  for  $\beta_R$ .

field distribution with localization at the  $\epsilon_3$ - $\epsilon_m$  interface. This is usually identified as the Fano mode due to the mixing of the two surface plasmons associated with the two film boundaries, in the limit  $h \rightarrow \infty$ . As  $h \rightarrow h_{c0}$  with  $h > h_{c0}$ , the fields penetrate progressively deeper into medium  $\epsilon_1$  becoming progressively more like uniform plane waves propagating parallel to the surface, but retaining a slight tilt toward the surface in order to compensate for loss in the metal. As  $h$  decreases below  $h_{c0}$ , the tilt angle increases and more energy is supplied to the wave than is needed to compensate for loss. As a result, the field localized in  $\epsilon_3$  grows with propagation distance.

The behavior near  $h_{c0}$  is complicated. For the plane-wave condition,  $\beta_R$  actually falls a small distance below  $(\epsilon_1)^{1/2}k_0$ . [If  $\epsilon_I = 0$ , the plane-wave condition corresponds to  $\beta_R = (\epsilon_1)^{1/2}k_0$ .] For  $h < h_{c0}$ , a growing wave solution is obtained for a region of  $\beta_R > (\epsilon_1)^{1/2}k_0$  (even in the limit  $\epsilon_I \rightarrow 0$ ). Such results indicate that the concept of the light line for separating radiative and nonradiative regions is not entirely compelling.

#### D. Variable $\epsilon_3/\epsilon_1$ : Fixed frequency

In this section we trace the four solutions through the material parameter range connecting the regions  $(\epsilon_3)^{1/2} = 1.5$  and  $(\epsilon_3)^{1/2} = 1.9$ . The upper branch solutions,  $a_b$  and  $a_l$  do not change character when  $(\epsilon_3)^{1/2}$  is varied from 1 to 2.0. As  $\epsilon_3 \rightarrow \epsilon_1$ , the  $\beta$  for the leaky wave solutions remains close to  $\beta_1(\infty) \simeq \beta_3(\infty)$  down to progressively thinner films. For  $\epsilon_3 = \epsilon_1 - \Delta$ , where  $\Delta$  is very small, the solutions track  $\beta_1(\infty)$  down to  $\Delta h$  at which point the  $\beta$  diverges rapidly with further decrease in  $h$ . For  $\Delta \rightarrow 0$ ,  $\beta \rightarrow \beta_1(\infty) = \beta_3(\infty)$ .

The nonradiative-growing wave branch is continuous over the full range  $\epsilon_3 = \epsilon_1 \rightarrow 1.0$ . Figure 9 illustrates  $h_{c0}$  as a function of  $\epsilon_3$ . For  $\beta_R \geq (\epsilon_1)^{1/2}k_0$ , this is the Fano (symmetric) mode branch. For  $\beta_R < (\epsilon_1)^{1/2}k_0$  this branch takes on the character of a Brewster mode, as noted before.

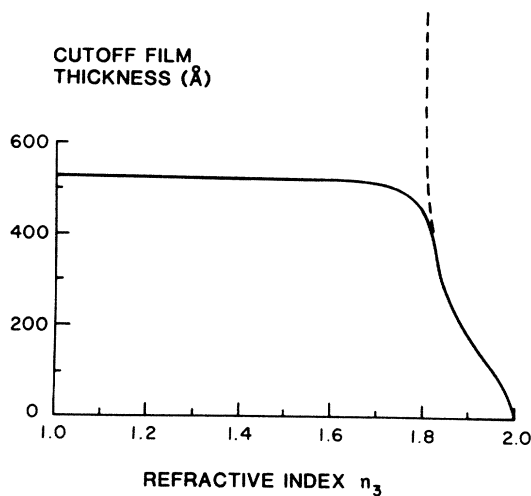


FIG. 9. Cutoff film thickness  $h_{c0}$  as a function of variable refractive index  $(\epsilon_3)^{1/2}$  for  $(\epsilon_1)^{1/2} = 2.0$ . The dashed and solid lines correspond to  $\epsilon_I = 0$  and  $\epsilon_I = +0.53$  with  $\epsilon_R = 19$  and  $\lambda = 0.633 \mu\text{m}$ .

This change in character of the solutions is evident in a number of ways. Consider first the case  $\epsilon_I = 0$ . At cutoff,  $\beta_R = (\epsilon_1)^{1/2}k_0$ ,  $S_1 = 0$ ,  $S_3 = (\epsilon_1 - \epsilon_3)^{1/2}k_0$ , and  $S_2 = ik_0(\epsilon_R + \epsilon_1)^{1/2}$ . Therefore, from the dispersion relation

$$h_{c0} = \frac{1}{k_0(\epsilon_1 + \epsilon_R)^{1/2}} \ln \left[ \frac{\epsilon_3(\epsilon_R + \epsilon_1)^{1/2} + \epsilon_R(\epsilon_1 - \epsilon_3)^{1/2}}{\epsilon_3(\epsilon_R + \epsilon_1)^{1/2} - \epsilon_R(\epsilon_1 - \epsilon_3)^{1/2}} \right] \quad (15)$$

and

$$1 \geq \frac{(\epsilon_1 - \epsilon_3)^{1/2} \epsilon_R}{(\epsilon_R + \epsilon_1)^{1/2} \epsilon_3} \quad (16)$$

must be satisfied for a finite  $h_{c0}$ . Equation (16) defines the smallest value of  $\epsilon_3$  for which a nonradiative mode can exist in the absence of dissipative loss. A plot of Eq. (15) is shown in Fig. 10. If  $\epsilon_I > 0$ , Eq. (6), with  $\beta_I = S_{1I} = S_{3I} = 0$ , predicts the cutoff thickness, and the inclusion of loss leads to a finite  $h_{c0}$  for all values of  $\epsilon_3$ . For  $\beta_3(\infty) \geq (\epsilon_1)^{1/2}k_0$ , the cutoff thickness varies with  $\epsilon_R$ , but only very weakly with  $\epsilon_I$ . However, for  $(\epsilon_1)^{1/2}k_0 > \beta_3(\infty)$ , the reverse holds, i.e.,  $h_{c0}$  varies strongly with  $\epsilon_I$  (Fig. 10), but not with  $\epsilon_R$ . Clearly, for  $\beta_3(\infty) > (\epsilon_1)^{1/2}k_0$  we have a surface-plasmon polariton mode, and for  $(\epsilon_1)^{1/2}k_0 > \beta_3(\infty)$  this is a Brewster type wave (because of its strong dependence on  $\epsilon_I$ ).

The field distributions also change when the equality given by Eq. (16) is crossed. Plotted in Fig. 11 is the mode attenuation and penetration depth into medium  $\epsilon_1$  as a function of  $\epsilon_3$  for thin metal films with  $\Delta h = 20$  and  $100 \text{ \AA}$  above  $h_{c0}$ . When  $\beta_R$  is decreased through  $(\epsilon_1)^{1/2}k_0$ , the penetration depth increases by orders of magnitude. When  $\beta_3(\infty) > (\epsilon_1)^{1/2}k_0$ , the fields are tightly bound because they rely on  $\epsilon_R > 0$  for their nonradiative character. The corresponding field distributions are shown in Fig. 12. When  $(\epsilon_1)^{1/2}k_0 > \beta_3(\infty)$ , the existence of dissipation is responsible for the nonradiative nature of the wave, and because  $\epsilon_R \gg \epsilon_I$ , the waves are not tightly coupled to the film.

The lower branch radiative mode  $s_l$  also varies smooth-

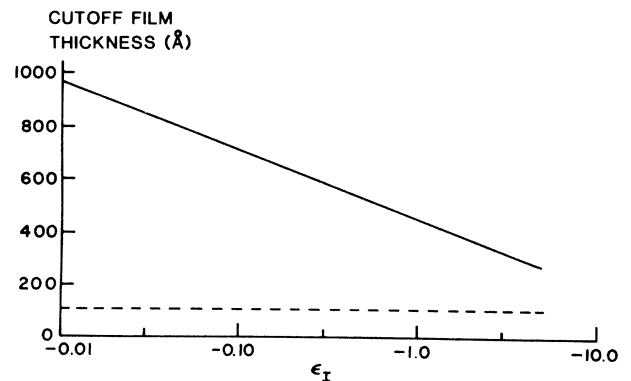


FIG. 10. Cutoff film thickness versus imaginary component of dielectric constant ( $\epsilon_I$ ) for the symmetric bound mode with  $(\epsilon_1)^{1/2} = 2.0$ ,  $(\epsilon_3)^{1/2} = 1.9$  (dashed line), and  $(\epsilon_1)^{1/2} = 2.0$ ,  $(\epsilon_3)^{1/2} = 1.5$  (solid line).



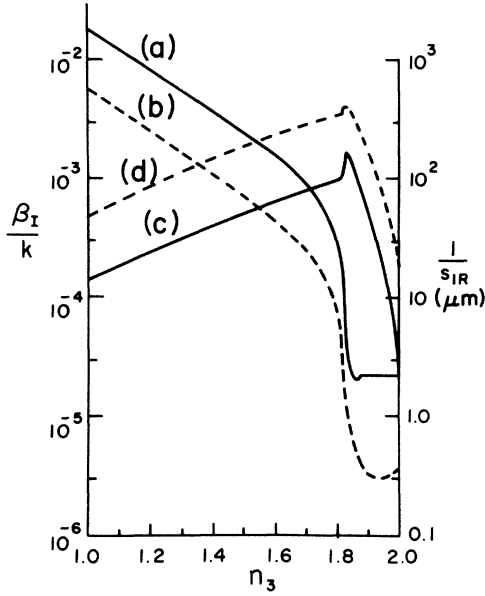


FIG. 11. Normalized attenuation and field penetration depth into medium  $\epsilon_1$  for film thickness 20 Å (solid line) and 100 Å (dashed line) above the cutoff thickness for the symmetric nonradiative mode. (a) and (b) refer to the penetration depth; and (c) and (d) to the attenuation.

ly with  $\epsilon_3$ . As  $\epsilon_3 \rightarrow \epsilon_1$ , the behavior is the same as that discussed for  $a_l$ , with the difference that  $\beta_R$  decreases as  $h \rightarrow 0$  (instead of increasing as was the case for  $a_l$ ). For  $(\epsilon_1)^{1/2}k_0 > \beta_3(\infty)$ , the radiation field is strongly peaked in direction over the full range of  $h$ .

The usual terminology<sup>1</sup> is to call  $a_b$  and  $s_b$  the Fano

modes for  $\beta_3(\infty) > (\epsilon_1)^{1/2}k_0$ , and  $a_b$  and  $s_l$  the Fano modes for  $\beta_3(\infty) < (\epsilon_1)^{1/2}k_0$ . Our analysis shows that  $s_b$  and  $s_l$  belong to different branches of the dispersion curves and probably should not both be called Fano modes.

## V. WAVELENGTH DEPENDENCE OF MODE SOLUTIONS

In the two preceding sections we discussed modes guided by thin, lossy silver films at the wavelength  $\lambda = 0.633 \mu\text{m}$  (He-Ne). This corresponds to the case  $\omega\tau \gg 1$ , where  $\tau$  is the relaxation time associated with Drude damping in the free-electron-gas model for  $\epsilon_m$ , i.e.,<sup>38</sup>

$$\epsilon_m = 1 - \frac{\omega_p^2}{\omega(\omega - i/\tau)}. \quad (17)$$

In this section we examine the same material system with  $\lambda = 10.6 \mu\text{m}$  (CO<sub>2</sub> laser) which corresponds to  $\omega\tau \approx 2$ . The wavelength dependence of the nonradiative symmetric mode is also evaluated for two metal thicknesses for  $\lambda$  varying from 0.5 to 15  $\mu\text{m}$ .

### A. CO<sub>2</sub> laser wavelength

The solutions for a symmetric structure  $\epsilon_1 = \epsilon_3$  at  $\lambda = 10.6 \mu\text{m}$  are identical in structure, dispersion, etc., to those discussed for  $\lambda = 0.633 \mu\text{m}$ . However, the parameter range over which  $\beta_R$  corresponds to a nonradiative symmetric wave, that is  $0.5k_0\epsilon^{3/2}\epsilon_R/|\epsilon_m|^2$ , is reduced drastically because of the large values attained by  $\epsilon_m(-4300 - 1800i)$ .<sup>39</sup> Furthermore, the asymptotic ( $h \rightarrow \infty$ ) attenuation, which scales the thin film loss, i.e.,  $\beta_l = \epsilon^{3/2}k_0\epsilon_l/2|\epsilon_m|^2$ , is also reduced from the  $\lambda = 0.633$

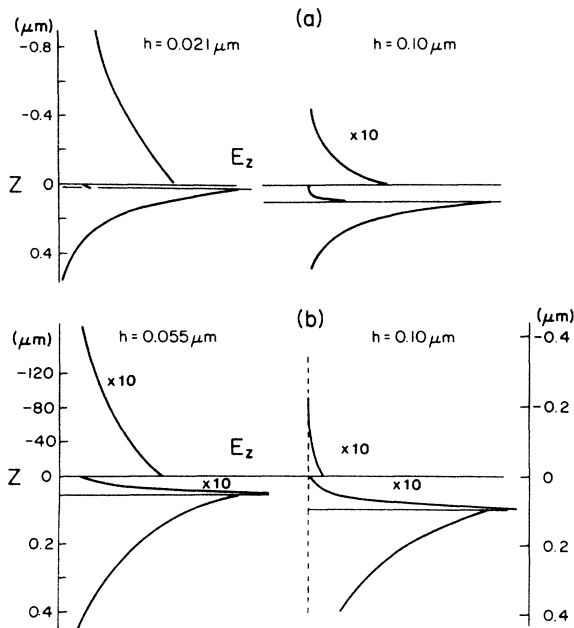


FIG. 12. Field distributions ( $E_z$ ) for the symmetric bound mode for (a)  $(\epsilon_1)^{1/2} = 2.0$  and  $(\epsilon_3)^{1/2} = 1.9$ ; (b)  $(\epsilon_1)^{1/2} = 2.0$  and  $(\epsilon_3)^{1/2} = 1.5$ . Film thicknesses 30 Å above cutoff were chosen.

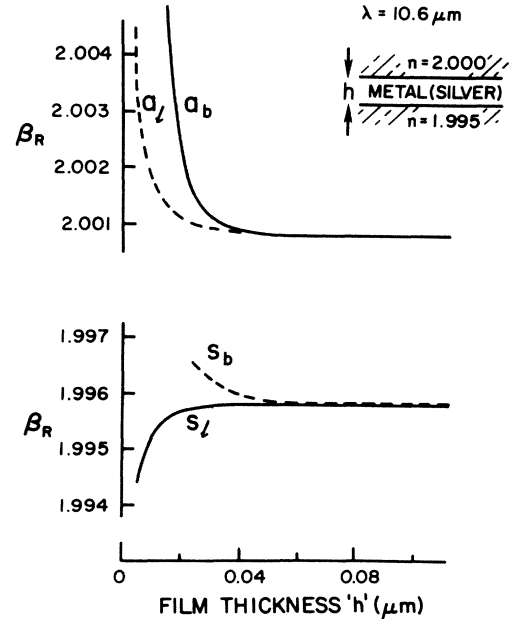


FIG. 13. Dispersion in  $\beta_R$  with thickness for the modal solutions for  $\lambda = 10.6 \mu\text{m}$ ,  $(\epsilon_1)^{1/2} = 2.0$ , and  $(\epsilon_3)^{1/2} = 1.995$ .  $s$  and  $a$  refer to the symmetric (lower) and antisymmetric (upper) branches, respectively.

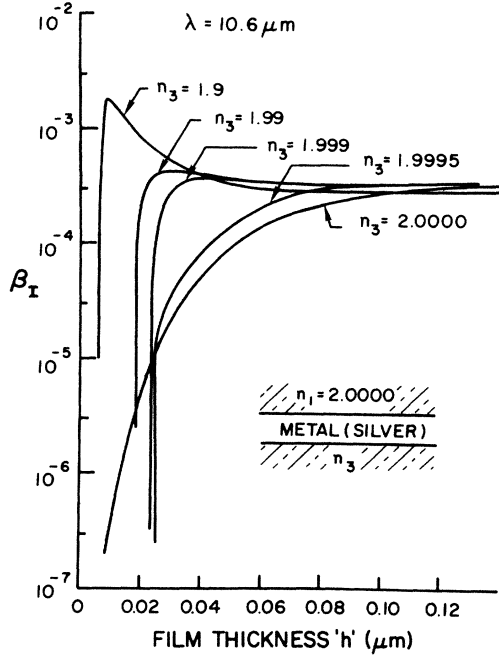


FIG. 14. Normalized attenuation constant versus film thickness for  $(\epsilon_1)^{1/2} = n_1 = 2.0$  and a variety of values for  $(\epsilon_3)^{1/2} = n_3$  at  $\lambda = 10.6 \mu\text{m}$ .

$\mu\text{m}$  cases.

Some of the changes in the waves guided by the asymmetric  $\epsilon_1 \neq \epsilon_3$  structure are more interesting. For the case  $\beta_3(\infty) > (\epsilon_1)^{1/2}k_0$ , the dispersion and attenuation with film thickness looks essentially like Fig. 8, with the values scaled as discussed above for the symmetric case. The range in  $\epsilon_3$  over which these solutions occur, as expressed by Eq. (16), is very limited and constitutes a very small fraction of the region  $\epsilon_1 \geq \epsilon_3 \geq 1.0$ . The dispersion relations for  $(\epsilon_3)^{1/2} = 1.995$  [ $(\epsilon_1)^{1/2}k_0 > \beta_3(\infty)$ ] are shown in Fig. 13. The behavior of the lower-branch nonradiative mode  $s_b$  differs from that found in Fig. 6. The cutoff thickness is reduced to  $\approx 240 \text{ \AA}$  and the wave vector  $\beta_R$  undergoes substantial dispersion with  $h$ . As predicted in Fig. 10, this decrease in  $h_{c0}$  is a consequence of the relatively large value of  $\epsilon_I$ .

A plot of attenuation versus film thickness with variable  $(\epsilon_3)^{1/2}$  (Fig. 14) reveals some interesting differences.  $h_{c0}$  increases until the limit of Eq. (16) is reached and then decreases, in contrast to the  $\lambda = 0.633 \mu\text{m}$  case where it remains approximately a constant. The cutoffs are still characterized by  $\beta_I \rightarrow 0$ , but the range of thickness over which  $\beta_I$  decreases becomes progressively smaller. In fact, maxima in attenuation occur due to increased upward dispersion in  $\beta_R$  with decreasing  $h$ .

#### B. Wavelength dependence

It is clear from the preceding discussion that the bound symmetric modes should exhibit an interesting wavelength dependence. For symmetric structures, the attenuation is low; thus long (and potentially useful) propagation distances appear possible. Furthermore, when the symmetric mode occurs in an asymmetric structure, it takes on two

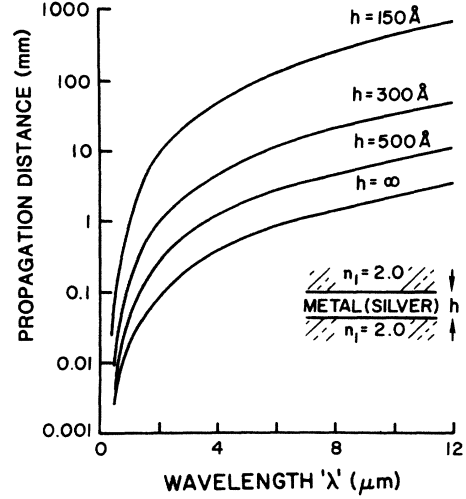


FIG. 15. Surface-polariton propagation distance versus wavelength for a symmetric structure [ $(\epsilon_1)^{1/2} = (\epsilon_3)^{1/2} = 2.0$ ] for a number of different metal film thicknesses.

distinctive forms which depend on dissipation ( $\epsilon_I$ ) in the metal, which in turn varies approximately as  $\lambda^3$ .

The wavelength dependence of the propagation distance (energy), mode penetration depth into the medium  $\epsilon_1$  and the parameter  $\beta_R - (\epsilon_1)^{1/2}k_0$  are shown in Figs. 15 and 16. To generate these curves we assumed Eq. (17) for the dielectric constant with  $\omega_p = 1.29 \times 10^{16} \text{ rad/s}$  and  $\tau = 1.25 \times 10^{-14} \text{ s}$ .

The most salient feature of Fig. 15 is the large propagation distances which can be achieved in the infrared. For  $\lambda > 1 \mu\text{m}$ , a distance greater than 1 mm is predicted for a 150  $\text{\AA}$  thick film. Given the cubic dependence on refrac-

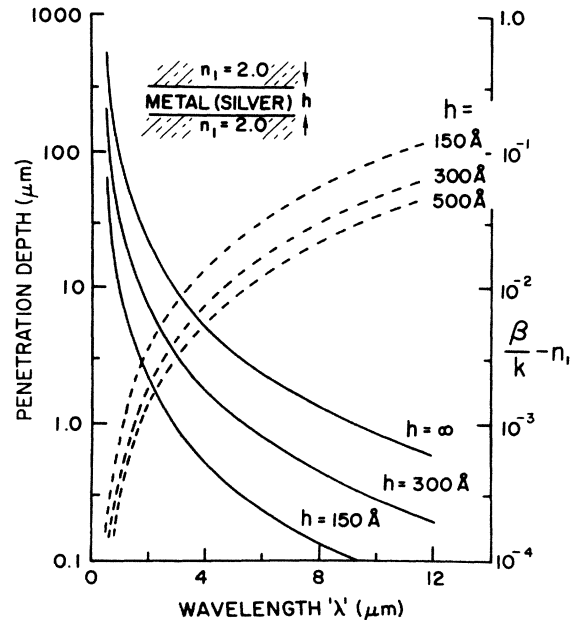


FIG. 16. Penetration depth into medium  $\epsilon_1$  and the difference between  $\beta_R$  and its mode cutoff value [ $(\epsilon_1)^{1/2}k_0$ ] for a symmetric structure ( $\epsilon_1 = \epsilon_3 = 4.0$ ) versus wavelength for a number of different metal film thicknesses.

tive index [Eq. (10)], the loss will be a factor of  $\simeq 4$  less for  $\sqrt{\epsilon} = 1.5$ . Furthermore, out at  $\lambda = 10.6 \mu\text{m}$ , multicenter distances are possible.

The reasons for these long propagation distances are evident in Fig. 16. As wavelength increases, the maximum separation of  $\beta_R$  from  $\sqrt{\epsilon}k_0$  decreases and the fields penetrate progressively deeper into the media  $\epsilon_1$ . For example, for  $h \simeq 150 \text{ \AA}$  at  $\lambda = 10.6 \mu\text{m}$  the waves penetrate  $\simeq 20$  optical wavelengths into each medium. The coupling to the film is weak and small material inhomogeneities can lead to scattering losses. In terms of utilizing these modes, wavelengths in the range  $2\text{--}5 \mu\text{m}$  appear ideal since the propagation distances are useful ( $1\text{--}100 \text{ mm}$  for  $h \simeq 150 \text{ \AA}$ ) and the confinements are in the  $1\text{--}4$  wavelength range.

We have also calculated the penetration depth (energy) and the propagation distance (energy) for the nonradiative symmetric wave as a function of wavelength for two film thicknesses with  $(\epsilon_1)^{1/2} = 2.0$  and  $(\epsilon_3)^{1/2} = 1.9$ . The results shown in Figs. 17 and 18 illustrate dramatically the effects of wavelength on these waves.

The two film thicknesses investigated show markedly different behavior for the nonradiative mode with wavelength. For the  $200 \text{ \AA}$  thick film, a tightly bound mode is maintained with increasing wavelength until the limit defined by Eq. (16) is reached. As equality is approached, the attenuation drops to zero and the penetration depth diverges. The weakly bound version appears for wavelengths above  $\simeq 4.65 \mu\text{m}$  and is characterized by very deep penetration depths into medium  $\epsilon_1$ . In contrast to this, a smooth transition between these two regimes is observed for the  $500 \text{ \AA}$  thick film. The mode remains tightly bound up to  $\lambda \simeq 0.9 \mu$  at which point it approaches cutoff as defined by Eq. (16). However, before it reaches cutoff it changes character to a weakly bound mode and both the penetration depth and the attenuation go through a maximum and minimum respectively. For further increases

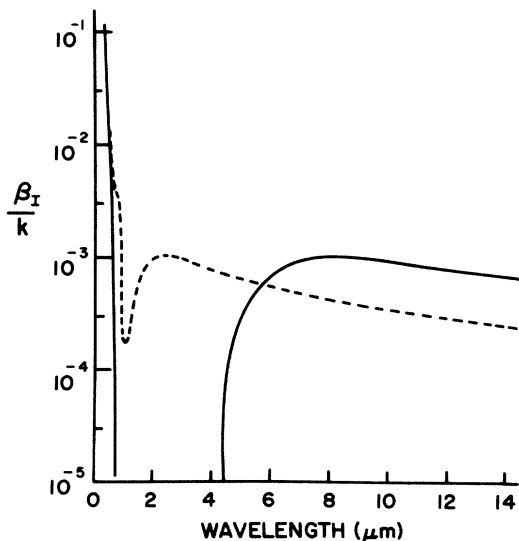


FIG. 17. Normalized attenuation for the symmetric nonradiative mode versus wavelength for the asymmetric structure  $(\epsilon_1)^{1/2} = 2.0$ ,  $(\epsilon_3)^{1/2} = 1.9$ . The solid line is for  $h = 200 \text{ \AA}$  and the dashed line for  $h = 500 \text{ \AA}$ .

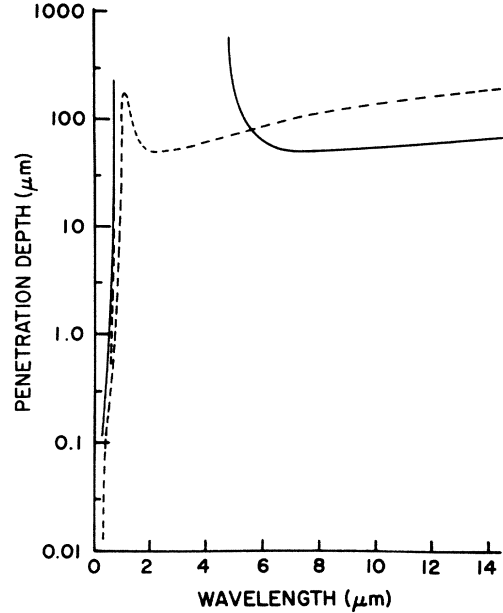


FIG. 18. The surface-polariton penetration depth into medium  $\epsilon_1$  for the asymmetric structure  $(\epsilon_1)^{1/2} = 2.0$ ,  $(\epsilon_3)^{1/2} = 1.9$  versus wavelength for the symmetric nonradiative mode. The solid line is for  $h = 200 \text{ \AA}$ , the dashed line for  $h = 500 \text{ \AA}$ .

in wavelength, the salient feature is the increase in propagation distance and penetration depth associated with the rapid increase in  $\epsilon_1$ .

## VI. DISCUSSION

### A. Summary of solutions

In the preceding sections we have outlined the solutions to the dispersion relations for waves guided by thin metal films and discussed their physical significance. For symmetric structures, there are four significant solutions. Two are nonradiative and correspond to the well-known Fano modes. The other two are both leaky in nature, and correspond to a surface plasmon guided by one or the other dielectric-metal interface. Their fields decay exponentially across the metal film and they couple to a broad spectrum of radiation fields in one of the dielectric media. All four solutions are also found for dissimilar bounding media.

The asymmetric structure solutions come in pairs, each of which contains a nonradiative wave (with a range of thickness over which a growing wave occurs) and a leaky (radiative) solution for a total of four solutions. Each pair of solutions is characterized by energy localized in an exponentially decaying field at one dielectric-metal film boundary. As the film thickness  $h \rightarrow \infty$ , the two waves in each pair become degenerate.

The behavior of the solutions which are asymptotic to  $\beta_1(\infty)$  [Eq. (8)] is straightforward for all values of the ratio  $\epsilon_3/\epsilon_1 < 1$ . The antisymmetric radiative branch persists in the same basic form, as does the nonradiative branch. For the latter, dispersion occurs with decreasing film thickness and the metal film carries progressively more of

the wave energy, with the result that the attenuation increases due to increased dissipation. The radiative solution, on the other hand, disperses less with thickness and hence has a smaller attenuation than the bound mode, despite the additional radiative loss.

The two solutions asymptotic (as  $h \rightarrow \infty$ ) to  $\beta_3(\infty)$  exhibit a more varied behavior depending on whether or not  $\beta_3(\infty)$  is larger than  $(\epsilon_1)^{1/2}k_0$ . The radiative branch produces a highly directional radiation pattern for all  $h$  if  $(\epsilon_1)^{1/2}k_0 > \beta_3(\infty)$ . If  $\beta_3(\infty)$  increases past  $(\epsilon_1)^{1/2}k_0$ , the range of thickness ( $0 < h < h'$ ) over which a directional radiation pattern is obtained decreases. For  $h > h'$ , no sharp peak is predicted; the total radiated power decreases and the angular width increases with increasing  $h$ . The detailed behavior in this region is complicated, cannot be summarized easily, and the reader is directed to Sec. IV for details.

The second of the two dispersion curves asymptotic to  $\beta_3(\infty)$  is divided into two thickness domains by a cutoff thickness  $h = h_{c0}$ . For  $h > h_{c0}$  nonradiative solutions are obtained. When  $h < h_{c0}$ , fields localized at the  $\epsilon_3 - \epsilon_m$  boundary are still obtained, but in this case they are coupled to an angular spectrum of incoming radiation fields in the higher index dielectric. For  $(\epsilon_1)^{1/2}k_0 > \beta_3(\infty)$ , this angular spectrum is sharply peaked; for  $\beta_3(\infty) > (\epsilon_1)^{1/2}k_0$  it is peaked only for very thin films, otherwise it is broad.

### B. Spatial transients

The leaky (radiative) branches  $a_l$  and  $s_l$  have the characteristics of spatial transients. Mathematically, the fields grow exponentially with distance from the metal film into the dielectric into which the wave radiates. As shown in detail in Sec. IV, such solutions only have physical significance over a limited range  $x$  (propagation direction) and  $z$  (depth into the radiation medium). For  $\beta_R \leq (\epsilon_1)^{1/2}k_0$ , the radiation pattern has a narrow angular spectrum. This coincides with the well-known "leaky Fano mode." When  $\beta_R > (\epsilon_1)^{1/2}k_0$  the radiation pattern is not sharp; instead radiation occurs into a broad continuum of plane waves. This is the case for the  $a_l$  branch, as well as for the  $\beta_R > (\epsilon_1)^{1/2}k_0$  portion of the  $s_l$  branch. These solutions have not been discussed in detail before, presumably because they fall on the nonradiative side of the  $\epsilon_1$  light line.

### C. Origin of solutions

The fact that there are four useful solutions to the dispersion relations in total can be understood in terms of the solutions for a single interface between a metal and a dielectric. As discussed in Sec. II, there are two solutions for that case. For the usual surface plasmon case the fields decay exponentially away from the boundary into both media. In the second case, the fields grow exponentially with distance from the boundary into both media. Traditionally these are rejected as unphysical, because they do not satisfy the boundary conditions at infinity. However, these waves are important in the larger context of leaky waves, which can be physically meaningful over limited regions of space only, but are uninteresting and can be neglected if there is no field localization.

The solutions for the metal film case correspond to all reasonable combinations of the two solutions associated with each metal interface. We illustrate this for  $\epsilon_1 = \epsilon_3$ . The two bound modes (Fano) are symmetric and antisymmetric combinations of the usual single-interface surface plasmon modes. For the antisymmetric modes, as the film thickness goes to zero,  $S_{2R}$  must become large enough for the field to decay rapidly inside the metal so that a field zero can occur within the film. Hence  $\beta_R$  diverges. The leaky waves are combinations of the  $SP_1$  or  $SP_3$  surface plasmons, and the exponentially growing solutions at the opposite interface. In this case we believe them to be physically meaningful because there is strong field localization in one of the dielectric media and the attenuation is multiwavelength.

It is noteworthy that for  $\beta_3(\infty) < (\epsilon_1)^{1/2}k_0$  one of the modes traditionally labeled Fano is actually a combination of  $SP_3$  and a solution characterized by an exponentially growing field at the  $\epsilon_1$  boundary.

### D. Dissipationless limit ( $\epsilon_I \rightarrow 0$ )

This limit is usually used to identify those solutions which are physically significant, i.e., a "mode." In this limit, one can employ normal-mode expansions which satisfy power orthogonality relations to describe the total field at any point in space. It is also usually stated that only normal modes can be excited in an experiment and hence have physical significance. Because some of our solutions do not satisfy all of these criteria, we wish to examine these concepts further. In our opinion, the critical question is whether a wave can be excited (or launched), and whether it interacts with other waves, etc. We shall address this question later.

We now examine the nature of the solutions to the dispersion relations for vanishingly small values of  $\epsilon_I$ . In particular we examine the situation for asymmetric structures. For  $a_b$ ,  $\beta_I$ ,  $S_{1I} = 0$ , and the mode structure persists for the antisymmetric branch. The leaky solution  $a_l$  is also characterized by  $\beta_I$ ,  $S_{1I}$ ,  $S_{3I} = 0$ . Although Eqs. (14) and (15) both predict no power loss via radiation fields, the exponential growth character of the fields in  $\epsilon_3$  persists. Therefore, for  $\epsilon_I = 0$ , the branch  $a_l$  has no apparent physical interpretation. However, if we consider any finite value of  $\epsilon_I$ , no matter how small, the interpretation of the  $a_l$  branch is clear. The smaller the radiative loss rate, the larger the effective aperture. Small  $\epsilon_I$  thus leads to nothing more than a spatial transient with a long "time" (length) constant. As  $\epsilon_I$  approaches zero, the effective aperture becomes too large for experimental study. Thus we conclude that the  $a_l$  branch becomes experimentally impractical as  $\epsilon_I \rightarrow 0$ , not physically insignificant.

The  $s_b$  branch has some interesting aspects in the limit  $\epsilon_I = 0$ . For  $h > h_{c0}$ , which requires  $\beta_3(\infty) > (\epsilon_1)^{1/2}k_0$ ,  $\beta_I$ ,  $S_{1I}$ ,  $S_{3I} = 0$ , and the solution is the well-known symmetric Fano mode.<sup>1</sup> For  $h < h_{c0}$ , there are two regimes. Between  $h_{c0}$  and  $h' > 0$  there is a region in which  $S_{1I}$ ,  $S_{3I}$ ,  $\beta_I > 0$  and the fields grow exponentially into the  $\epsilon_1$  medium. To understand the physical meaning of this solution, we must examine it for very small, but nonzero, values of  $\epsilon_I$ . It is then clear that the corresponding waves grow

slowly with distance along the structure, driven from the high-index dielectric by an incoming narrow angular spectrum of plane waves. From  $0 < h < h'$ ,  $\beta_I < 0$ ,  $S_{1I} < 0$ , and  $S_{3I} > 0$  and the fields which grow exponentially into  $\epsilon_1$  signify a mode growing with propagation distance, i.e., pumped by radiation fields incident from  $\epsilon_1$ . When  $\beta_3(\infty) < (\epsilon_1)^{1/2}k_0$ , only growing wave solutions are obtained.

The  $s_I$  branch also has interesting characteristics when  $\epsilon_I = 0$ . For  $\beta_3(\infty) < (\epsilon_1)^{1/2}k_0$ ,  $\beta_I > 0$ ,  $S_{1I} > 0$ , and  $S_{3I} < 0$ . The attenuation characterized by  $\beta_I > 0$  is totally accounted for by the radiation loss into medium  $\epsilon_1$  and the wave-front tilt and exponential growth into  $\epsilon_1$  are consistent with a leaky wave. For  $\beta_3(\infty) > (\epsilon_1)^{1/2}k_0$ , the wave-front tilt persists for  $0 < h < h'$ . If  $h > h'$ ,  $S_{1I} = S_{3I} = 0$  and the branch has no apparent physical significance.

These results show, that for  $\epsilon_I = 0$ , the light line does indeed separate radiative and nonradiative regions of the dispersion curves. Hence leaky modes are forbidden when  $\beta_R > (\epsilon_1)^{1/2}k_0$ . It does not, however, exclude such modes for  $\epsilon_I > 0$ . The important criterion still is whether the modes can be excited or not, and whether they interact with other waves, etc.

### E. Wave launching

We now address the question of why all of these solutions have not been observed before, and which ones we expect can be observed. The answer to this question is intimately related to the problem of determining all the field constituents that form the complete solution for the field due to an arbitrary source located in a given geometry.

In our case, the geometry is that shown in the inset of Fig. 1. The best source to consider for this two-dimensional situation ( $\partial/\partial y \equiv 0$ ) is a line source in parallel to the  $y$  direction; this source may consist, for example, of a magnetic current flowing along  $y$ , or of continuous electric dipoles placed along  $y$  and pointing in the  $x$  direction. These currents play the role of a Green's function source. Any other source can then be synthesized by a suitable superposition of such line sources. A specific field constituent, e.g., any of the fields  $s_b$ ,  $s_I$ ,  $a_b$ , or  $a_I$  discussed above, can therefore be launched only if it can be excited by a line source because if that field constituent cannot be produced by that source, then no source can excite it. To explore these questions, we examine below the field due to a line source by using an analysis involving the representation of fields by means of the integrals in complex wave-number planes, which have often been used to resolve problems of this type. Due to constraints on the length of this paper, these aspects can be discussed here only briefly and the reader should refer to the literature<sup>40-42</sup> for details.

Without any loss of generality, we may assume that the line source is placed in the upper medium at  $x=0$  and  $z=-d$ . The field in that medium will then be given by  $\mathbf{H} = \hat{\mathbf{J}}\mathbf{H}$  with

$$\mathbf{H} = \mathbf{H}_i + \mathbf{H}_r, \quad (18)$$

where  $\mathbf{H}_i$  is the incident magnetic field, which is a cylindrical wave in this case, while  $\mathbf{H}_r$  is the reflected

field, which is given by

$$H_r = I \int_{-\infty}^{\infty} r(\beta) \frac{\exp[S_1(z-2d) - i\beta x]}{S_1} d\beta. \quad (19)$$

Here  $I$  is a constant proportional to the source intensity and the frequency dependence  $\exp(i\omega t)$  has been suppressed. The function  $r(\beta)$  is the reflection coefficient at the upper ( $z=0$ ) boundary for plane waves incident at an angle  $\theta$  given by

$$\beta = k_0(\epsilon_1)^{1/2} \cos \theta, \quad (20)$$

and it is understood that  $\theta$  may be complex. For the parallel polarized waves considered here, the remaining field components  $E_x$  and  $E_z$  can be found from Eqs. (2), (18), and (19).

The integration in Eq. (19) follows the path  $P$  along the real axis  $\beta_R$  of the complex  $\beta = \beta_R - i\beta_I$  plane shown in Fig. 19. To evaluate the integral in Eq. (19) and to determine the field constituents that result from such an integration, it is necessary to define the singularities of the integrand in the vicinity of the path  $P$ . Because of Eqs. (6), we have

$$S_1 = (\beta^2 - \epsilon_1 k_0^2)^{1/2}, \quad (21)$$

$$S_3 = (\beta^2 - \epsilon_3 k_0^2)^{1/2}. \quad (22)$$

Due to the square roots, branch points exist at  $\beta = \pm(\epsilon_1)^{1/2}k_0$  and  $\pm(\epsilon_3)^{1/2}k_0$ , so that branch cuts must be defined to analytically determine the values of  $S_1$  and  $S_3$  in the  $\beta$  plane. [Branch cuts are not needed for  $S_2$  because, as can be inferred from Eq. (5), the integrand is an

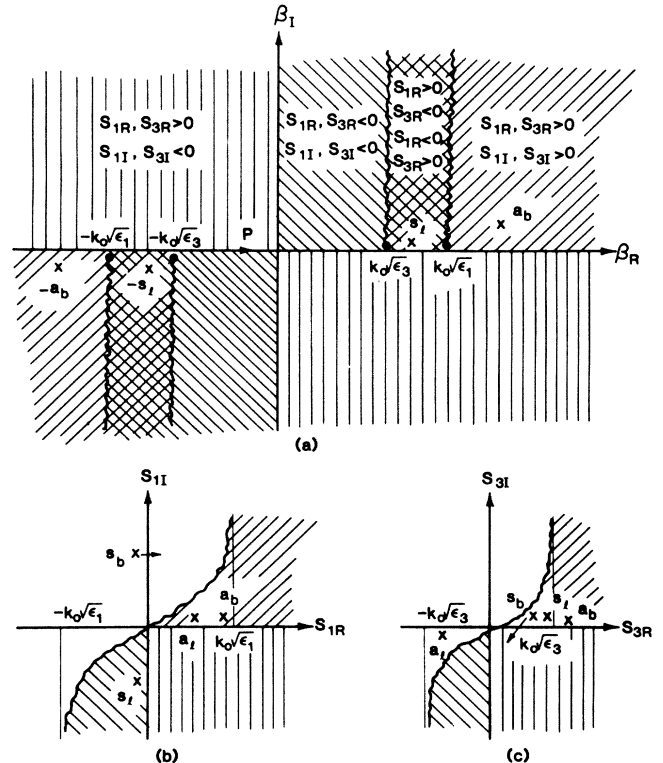


FIG. 19. Field solutions and singularities in (a) the complex  $\beta$  plane; (b) the complex  $S_1$  plane; (c) the complex  $S_3$  plane.

even function of  $S_2$ .] By invoking the familiar argument of small losses, the branch points are shown in Fig. 19(a) to be located slightly off the  $\beta$  axis, thus defining their relationship with respect to the path  $P$ . The branch cuts are then most conveniently chosen as shown by the wavy lines in Fig. 19. These four cuts imply that the complex  $\beta$  plane consists of four Riemann sheets, of which only one is shown in Fig. 19. As discussed further below, the path  $P$  can only occur on this (proper) sheet because the integrand in Eq. (19) is unbounded in the other (improper) sheets.

The complex  $S_1$  and  $S_3$  planes are also shown in Fig. 19, with wavy lines corresponding to the branch cuts chosen in the  $\beta$  plane. The proper sheet of the  $\beta$  plane is then defined so that its shaded portions correspond to the regions in the planes  $S_1$  and  $S_3$  that have the same shading. The unshaded portions of the  $S_1$  and  $S_3$  planes map into parts of the three other sheets of the  $\beta$  plane. We then note that the path  $P$  starts and ends in regions in which both  $S_{1R}$  and  $S_{3R}$  are positive, thus ensuring that the integrand in Eq. (19) is bounded as  $\beta_R \rightarrow \pm \infty$ . That would not be the case if  $P$  were in one of the other three sheets of the  $\beta$  plane, which explains why they are labeled "improper."

In addition to branch-point singularities, the integrand in Eq. (19) contains poles at points for which the reflectance function  $r(\beta)$  goes to infinity. These points are exactly those given by the field solutions discussed here because Eq. (7) can also be obtained by equating the denominator of  $r(\beta)$  to zero. We are concerned here mainly with poles of  $r(\beta)$  that are close to the  $\beta_R$  axis: poles located far away from that axis refer to fields that decay very rapidly along  $x$ , so that they are of negligible importance. Typical locations of such pertinent poles in the  $S_1$  and  $S_3$  planes are then shown by the crosses marked as  $s_b$ ,  $s_l$ ,  $a_b$ , and  $a_l$  solutions; note that the  $s_b$  solution is accompanied by an arrow indicating the change in location as that solution goes through the dip illustrated in Figs. 6 and 8.

If we now plot the above poles in the  $\beta$  plane, we see in Fig. 19 that only  $s_l$  and  $a_b$  solutions appear in the proper  $\beta$  sheet. The points for the  $s_b$  and  $a_l$  solutions appear in some of the other three sheets because they are located in unshaded regions of either the  $S_1$  or  $S_3$  planes. When evaluating the integrand along  $P$ , we therefore conclude that only  $s_l$  and  $a_b$  affect the integration result, so that only those solutions contribute field constituents to the total solution. Phrased differently, the integration along  $P$  can be carried out by deforming  $P$  into a different path, e.g., a semicircle at infinity. The result then consists of two continuous (radiation) spectra due to the integrations along two branch cuts, plus residue contributions due to poles that are located between the path  $P$  and the deformed path.<sup>43</sup> It is these residues that account for the fields given by  $s_l$  and  $a_b$  solutions, as expressed by Eqs. (1)–(3).

It might be argued that different choices of branch cuts for  $S_1$  and  $S_3$  would place  $s_b$  and  $a_l$  in the upper sheet of the integration plane  $\beta$  and thus provide pole residues from these two solutions. While this is correct, the uniqueness theorem requires that the result for the total field does not depend on the choice of the branch cuts.

When deforming  $P$  into a semicircle at infinity, the choice of cuts shown in Fig. 19 yields two continuous spectra and two residues that are well separated, i.e., they are distinct from each other in a phase plane. Hence they provide four different field constituents which can presumably be identified individually by an appropriate measurement. Any other choice of branch cuts could yield only the same measurable result; this implies that any pole residue due to either  $s_b$  or  $a_l$  will necessarily be masked and effectively suppressed by a field provided from a continuous spectrum due to a branch cut different from the ones shown in Fig. 19. This is analogous to the situation that exists for the Zenneck wave, which is associated with a pole located in the complex plane in a way similar to that of  $s_b$  and  $a_l$ . As has been finally resolved after a lengthy controversy,<sup>44</sup> the Zenneck wave does not appear as a distinct field contribution; at most, the Zenneck pole affects the total field by introducing a small perturbation when the pole is located close to the branch point. Similarly, even if solutions of the type  $s_b$  or  $a_l$  happen to be close to  $k_0(\epsilon_1)^{1/2}$  or  $k_0(\epsilon_3)^{1/2}$ , their effect on the total field will be negligibly small.

We therefore conclude that the Fano modes represented by  $s_l$  and  $a_b$  are physically admissible and launchable, as was also confirmed experimentally. However, fields of the form  $s_b$  and  $a_l$  cannot be sustained on the infinite three-media geometry discussed here.

#### F. End-fire excitation

We now propose a different method for selectively exciting surface polariton modes in asymmetric (or symmetric) structures. Consider injecting light into the sample using the "end-fire" configuration (well known in integrated optics)<sup>45</sup> shown in Fig. 20. The goal is to match the externally incident fields via masking techniques (tapered attenuators, spatial filters in the lens, etc.) to the field associated with the solution we are trying to generate. For example, near a mode cutoff, its fields penetrate much deeper into medium  $\epsilon_1$  than those of any other mode; it can therefore be preferentially excited. Although this approach is not  $\beta_R$  selective (such a prism coupler is), the appropriate wave-front tilt (and hence  $\beta_R$ ) is needed for the lower branch modes of Sec. IV B. For  $\lambda = 10.6 \mu\text{m}$ , the penetration depths are many optical wavelengths; lenses in the  $f1 \rightarrow f10$  range should be ap-

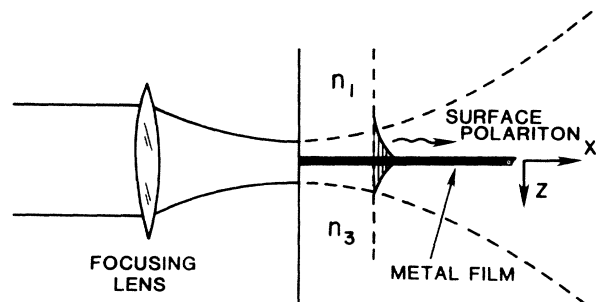


FIG. 20. "End-fire" coupling geometry for exciting surface plasmons.

appropriate. The expectation is that a solution to the dispersion relation should propagate without changing its field profile, which can then be observed after some propagation distance. Such an experiment also has its uncertainties. For example, all allowed modes are excited to a larger degree than with a prism coupler. Nevertheless, a well-designed experiment should cast some further light on the field distributions which can be propagated.

### G. Resonance interpretation

To this point we have been treating the various solutions to the dispersion relations as individual waves. Although we expect that the solutions can be propagated as discrete field distributions (if they can be launched), they can also be treated as different aspects of resonances at the two metal-dielectric interfaces.

For example, consider the  $s_b$  and  $s_l$  branches in Fig. 6. The wave-front tilts in medium  $\epsilon_1$  are into, and out of the film, respectively, for wave localized at the  $\epsilon_3$ - $\epsilon_m$  boundary. The solution tilted towards the surface ( $s_b$ ) can couple to incoming radiation fields, and the wave ( $s_l$ ) tilted away from the metal- $\epsilon_1$  interface generates outgoing (radiation) fields. The two branches, therefore, describe different aspects of the same resonance at the  $\epsilon_3$ - $\epsilon_m$  interface.

A similar argument can be applied to the other branches of solutions discussed in the paper. For example, consider the  $a_b$  and  $a_l$  solutions. The wave fronts are tilted towards and away from the film, respectively, to describe coupling (potential in the case of  $a_b$ ) to incoming and outgoing radiation fields. In fact if medium  $\epsilon_1$  is in the form of a thick film and coupling to incident plane waves is allowed, it is the  $a_b$  solution which couples.

This interpretation is supported by the value of  $\beta_l$  for the solution with the largest attenuation, relative to the  $\Delta\beta_R$  between waves describing the same resonance. In

each and every case,  $\beta_l > \Delta\beta_R$ , which verifies the mixed nature of the resonances. Furthermore, the field amplitude distributions inside the dielectric where the resonances occur (field enhancements associated with energy storage) are almost identical.

This interpretation can circumvent the problem of which modes are "physical," etc. In any practical sample geometry, it is the resonance which is physical. Whether the coupling of the resonance to incoming or outgoing radiation fields is important depends on the particular experiment, and for most cases both couplings occur. A viable conclusion is that all of the solutions described here are physically significant because they describe different aspects of the same resonance. We also note that all of the standard ATR calculations, etc., include both couplings by virtue of the fact that both incident and reflected (outgoing) plane waves are included.

The proliferation of waves discussed here should occur for any film which exhibits a dielectric constant of the form  $\epsilon = -\epsilon_R - i\epsilon_I$ . An example would be surface phonon polaritons<sup>2</sup> which involve the coupling of electromagnetic fields to vibrational resonances in the film. Another example is surface exciton polaritons,<sup>3</sup> which exist by virtue of the coupling of electromagnetic fields to hole-electron pairs in semiconductors. In these cases the film dielectric constants do not take on values as large as for metals and hence the appropriate film thicknesses will be much larger than for metals.

### ACKNOWLEDGMENTS

This research is supported by the U.S. Army Research Office under Contract No. DAAG-29-85-K-0026, by NASA under Contract No. NAG3-392, and by the U.S. Joint Services Electronics Program under Contract No. F49620-82-C-0084. The assistance of Mr. F. Y. Kou in clarifying some of the numerical results is acknowledged with thanks.

<sup>1</sup>See, for example, E. Burstein, A. Hartstein, J. Schoenwald, A. A. Maradudin, D. L. Mills, and R. F. Wallis, in *Polaritons, Proceedings of the First Taormina Research Conference on the Structure of Matter, Taormina, 1973*, edited by E. Burstein and F. De Martini (Pergamon, Oxford, 1974), p. 89, and references cited therein; P. Halevi, *Surf. Sci.* **76**, 64 (1978).

<sup>2</sup>D. N. Mirlin, in *Surface Polaritons, Electromagnetic Waves at Surfaces and Interfaces*, edited by V. M. Agranovich and D. L. Mills (North-Holland, Amsterdam, 1982), p. 3, and references cited therein.

<sup>3</sup>J. Lagois and B. Fischer, in *Surface Polaritons, Electromagnetic Waves at Surfaces and Interfaces*, edited by V. M. Agranovich and D. L. Mills (North-Holland, Amsterdam, 1982), p. 69, and references cited therein.

<sup>4</sup>G. N. Zhizhin, M. A. Moskalova, E. V. Shomina, and V. A. Yakovlev, in *Surface Polaritons, Electromagnetic Waves at Surfaces and Interfaces*, edited by V. M. Agranovich and D. L. Mills (North-Holland, Amsterdam, 1982), p. 93, and references cited therein.

<sup>5</sup>R. H. Ritchie, *Phys. Rev.* **106**, 874 (1957).

<sup>6</sup>E. A. Stern and R. A. Farrell, *Phys. Rev.* **120**, 130 (1960).

<sup>7</sup>See, for example, E. N. Economou, *Phys. Rev.* **182**, 539 (1969).

<sup>8</sup>K. L. Kliever and R. Fuchs, *Phys. Rev.* **153**, 498 (1967).

<sup>9</sup>R. H. Ritchie, *Surf. Sci.* **34**, 1 (1973), and references contained therein.

<sup>10</sup>J. Schoenwald, E. Burstein, and J. M. Elson, *Solid State Commun.* **12**, 185 (1973).

<sup>11</sup>J. D. McMullen, *Solid State Commun.* **17**, 331 (1975).

<sup>12</sup>D. L. Begley, D. A. Bryan, R. W. Alexander, R. J. Bell, and C. A. Goben, *Surf. Sci.* **60**, 99 (1970).

<sup>13</sup>For example, K. J. Krane and H. Raether, *Phys. Rev. Lett.* **37**, 1355 (1976).

<sup>14</sup>For example, N. Marschall, B. Fischer, and H. J. Queisser, *Phys. Rev. Lett.* **27**, 95 (1971).

<sup>15</sup>A. Otto, *Z. Phys.* **216**, 398 (1968).

<sup>16</sup>R. Bruns and H. Raether, *Z. Phys.* **237**, 98 (1970).

<sup>17</sup>A. S. Barker, Jr., *Phys. Rev. Lett.* **28**, 892 (1972).

<sup>18</sup>E. T. Arakawa, M. W. Williams, R. N. Hamm, and R. H. Ritchie, *Phys. Rev. Lett.* **31**, 154 (1974).

<sup>19</sup>W. H. Weber and S. L. McCarthy, *Appl. Phys. Lett.* **25**, 396

- (1974); Phys. Rev. B **12**, 5643 (1975).
- <sup>20</sup>A. B. Buckman and C. Kuo, J. Opt. Soc. Am. **69**, 343 (1979).
- <sup>21</sup>H. Kitajima, K. Hieda, and Y. Suematsu, J. Opt. Soc. Am. **70**, 1507 (1980).
- <sup>22</sup>F. Abeles and T. Lopez-Rios, Opt. Commun. **11**, 89 (1974).
- <sup>23</sup>G. C. Aers, A. D. Boardman, and P. Clark, Phys. Status Solidi B **85**, 171 (1978).
- <sup>24</sup>S. Hayashi, T. Yamada, and H. Kanamori, Opt. Commun. **36**, 195 (1981).
- <sup>25</sup>P. K. Tien, Rev. Mod. Phys. **49**, 361 (1977).
- <sup>26</sup>M. Fukui, V-C.Y. So, and R. Normandin, Phys. Status Solidi B **91**, K61 (1979).
- <sup>27</sup>D. Sarid, Phys. Rev. Lett. **47**, 1927 (1981).
- <sup>28</sup>Y. Kuwamura, M. Fukui, and O. Tada, J. Phys. Soc. Jpn. **52**, 2350 (1983).
- <sup>29</sup>J. C. Quail, J. G. Rabo, and H. J. Simon, Opt. Lett. **8**, 377 (1983).
- <sup>30</sup>A. E. Craig, G. A. Olson, and D. Sarid, Opt. Lett. **8**, 383 (1983).
- <sup>31</sup>H. Dohi, Y. Kuwamura, M. Fukui, and O. Tada, J. Phys. Soc. Jpn. **53**, 2828 (1984).
- <sup>32</sup>P. E. Ferguson, D. F. Wallis, and C. Hauvet, Surf. Sci. **82**, 255 (1979).
- <sup>33</sup>G. I. Stegeman, J. J. Burke, and D. G. Hall, Opt. Lett. **8**, 383 (1983).
- <sup>34</sup>T. Tamir and A. A. Oliner, Proc. IEEE (London), **110**, 310 (1963).
- <sup>35</sup>T. Tamir and A. A. Oliner, Proc. IEEE (London), **110**, 325 (1963).
- <sup>36</sup>J. J. Burke and N. S. Kapany, *Optical Waveguides* (Academic, New York, 1972).
- <sup>37</sup>V. Shah and T. Tamir, Opt. Commun. **12**, 113 (1977).
- <sup>38</sup>T. Hollstein, U. Kreibeg, and F. Leis, Phys. Status Solidi B **82**, 545 (1977).
- <sup>39</sup>A. P. Lenham and D. M. Treherne, J. Opt. Soc. Am. **56**, 683 (1966).
- <sup>40</sup>L. M. Brekhovskikh, *Waves in Layered Media* (Academic, New York, 1960), Chap. IV.
- <sup>41</sup>G. Tyras, *Radiation and Propagation of Electromagnetic Waves* (Academic, New York, 1969), Chap. 6.
- <sup>42</sup>L. B. Felsen and N. Marcuvitz, *Radiation and Scattering of Waves*, (Prentice-Hall, Englewood Cliffs, New Jersey, 1973), Chap. 5.
- <sup>43</sup>See, for example, T. Tamir, in *Electromagnetic Surface Modes*, edited by A. D. Boardman (Wiley, London, 1982), p. 543.
- <sup>44</sup>See, for example, A. Banos, Jr., *Dipole Radiation in the Presence of a Conducting Half-Space* (Pergamon, New York, 1966).
- <sup>45</sup>H. P. Hsu, A. F. Milton, and W. K. Burns, Appl. Phys. Lett. **33**, 603 (1978).